

## Supplementary Material

### **BiOBr/Bi<sub>4</sub>MoO<sub>9</sub> edge-on heterostructure with fast electron transport for efficient photocatalytic activity**

Gui Yang <sup>a</sup>, Yujun Liang <sup>a,\*</sup>, Jian Yang <sup>a</sup>, Kun Wang <sup>a</sup>, Zikang Zeng <sup>a</sup> and Zhuoran

Xiong <sup>a</sup>

<sup>a</sup> *Engineering Research Center of Nano-Geomaterials of Ministry of Education,  
Faculty of Materials Science and Chemistry, China University of Geosciences,  
Wuhan 430074, China*

**\*Corresponding author:** Tel: +86 27 67884814; fax: +86 27 67883733.

E-mail address: [yujunliang@sohu.com](mailto:yujunliang@sohu.com) (Yujun Liang)

## Experimental section

### Preparation of photocatalysts

Two synthesis processes were used to synthesize the (BiOBr/Bi<sub>4</sub>MoO<sub>9</sub>) heterojunctions.

(1) Molten salt-assisted synthesis process (Bi<sub>4</sub>MoO<sub>9</sub>). NaNO<sub>3</sub> with the eutectic point of 308 °C was employed as the molten salt, and the mass ratio of molten salts to raw materials was 8:1. Typically, 1.21 g of Bi(NO<sub>3</sub>)<sub>3</sub>·5H<sub>2</sub>O and 0.30 g Na<sub>2</sub>MoO<sub>4</sub>·2H<sub>2</sub>O were fully ground for about 15 min. Subsequently, the mixture was further grinded with 0.8499 g NaNO<sub>3</sub> for more than 30 min to form a well-dispersed mixture. The mixed powders were heated at 500 °C for 10 h in air. Finally, the obtained samples were treated with the hot deionized water and ethanol to remove NaNO<sub>3</sub>. Finally, the obtained samples were dried at 80 °C for 24 h.

(2) Surface chemical etching process (BiOBr/Bi<sub>4</sub>MoO<sub>9</sub>). The BiOBr/Bi<sub>4</sub>MoO<sub>9</sub> edge-on heterostructure was further fabricated by using a simple chemical etching strategy. Typically, 0.1 g of Bi<sub>4</sub>MoO<sub>9</sub> was dissolved in HNO<sub>3</sub> (30 mL, 0.5 mol L<sup>-1</sup>), termed as solution A. 0.8 g of KBr were dissolved in 10 mL de-ionized water, termed as solution B. Subsequently, solution B was dropwise added into solution A. After vigorously stirring for 30 min, the resultant samples were rinsed using the deionized water and ethanol, and then dried at 80 °C for further use.

## **Characterization**

Powder X-ray diffraction (XRD) data of the as-prepared samples were collected on an X-ray diffractometer (D8-FOCUS, Bruker, Germany) with Cu K $\alpha$  radiation ( $\lambda = 1.5418 \text{ \AA}$ ). The morphology and microstructure observation were examined by field emission scanning electron microscope (FE-SEM, SU8010, Hitachi, Japan) and transmission electron microscope (TEM, Tecnai G2 T20, FEI, America). Meanwhile, the energy-dispersive X-ray spectroscopy (EDS) spectra and elemental mapping images were collected in an EDAX Genesis, which was attached to the FE-SEM. X-ray photoelectron spectroscopy (XPS) measurement was performed on a Thermo Scientific Escalab 250X spectrometer equipped with an Al K $\alpha$  X-ray source. UV-vis diffuse reflectance spectra (DRS) were tested on an UV-2550PC spectrophotometer (Shimadzu Corporation, Japan), using BaSO<sub>4</sub> as the reflectance standard. The photoluminescence (PL) spectra of photocatalysts were measured by a fluorescence spectrometer (Fluoromax-4P, Horiba Jobin Yvon, New Jersey, USA), which was equipped with a 150 W xenon lamp as the excitation source.

## **Photocatalytic measurements**

The photocatalytic performances of all catalysts were measured by photodegradation of tetracycline (TC). The photocatalytic experiments were conducted in a multipath photochemical reaction system (PCX50B, Beijing Perfect Light Technology co., LTD). A 5 W white LED was used as a visible light source with the light intensity of 72.9 mW·cm<sup>-2</sup>. Typically, 20 mg samples were dispersed in 50 mL TC solution (10

mg/L) for photocatalytic activity tests. The residual concentration of TC was determined by UV-vis spectrophotometer at a maximum absorbance wavelength of 357 nm. In addition, the intermediates of residue TC were further analyzed on a HPLC-MS system (Agilent 1200 HPLC 6460A MS/MS, USA).

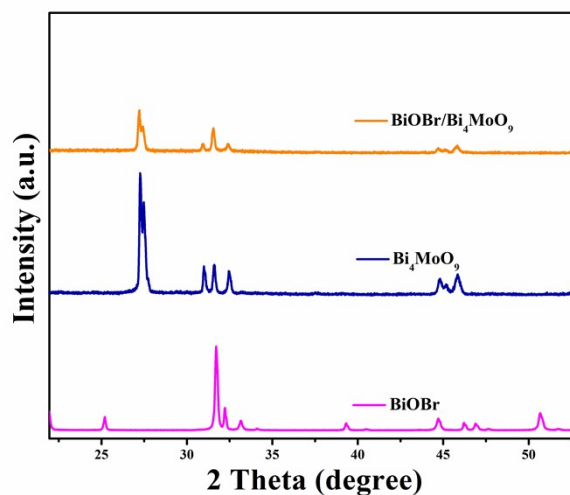


Fig. S1 The XRD patterns of as-obtained samples.

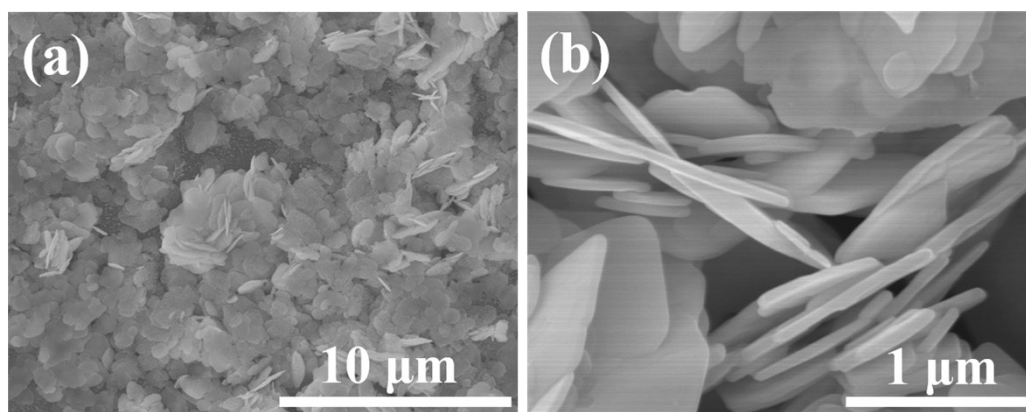


Fig. S2 (a) SEM images of pure BiOBr.

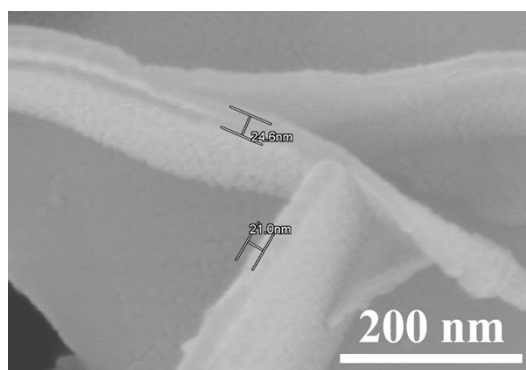


Fig. S3 (a) SEM image of BiOBr/Bi<sub>4</sub>MoO<sub>9</sub>.

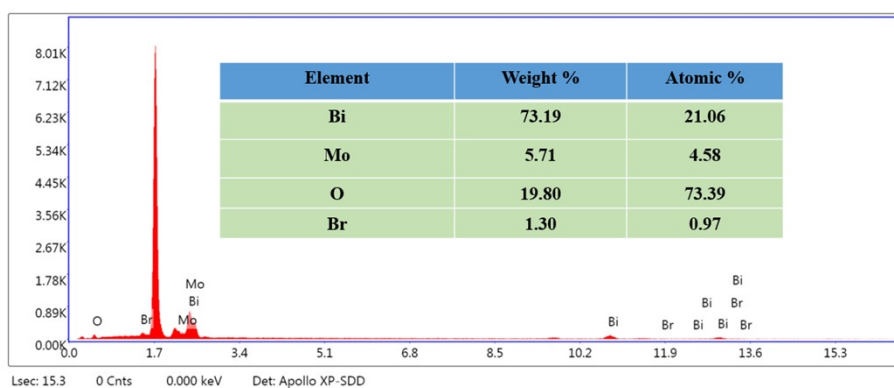


Fig. S4 EDS spectra of the BiOBr/Bi<sub>4</sub>MoO<sub>9</sub>.

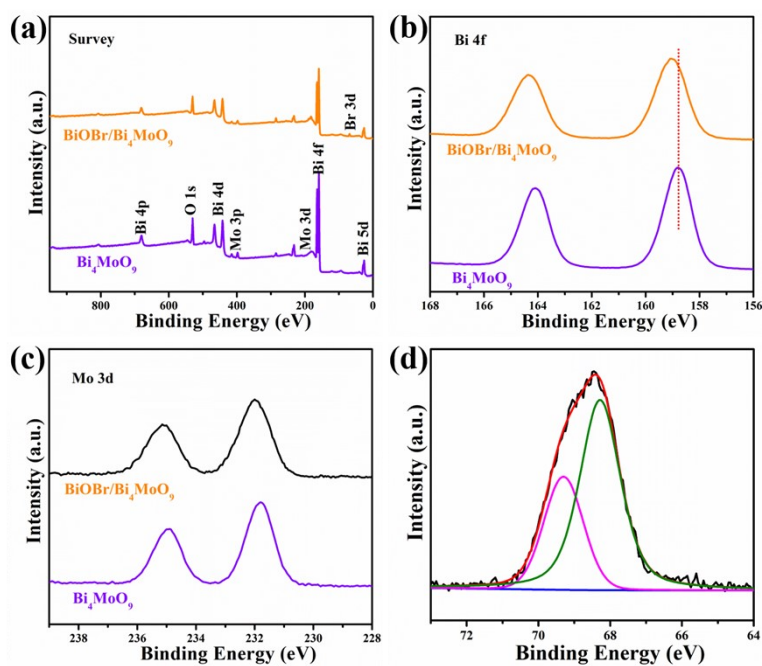


Fig. S5 XPS spectra of samples, full survey spectra (a), Bi 4f (b), Mo 3d (c) and Br 3d

(d).

XPS spectra of the  $\text{Bi}_4\text{MoO}_9$  and  $\text{BiOBr}/\text{Bi}_4\text{MoO}_9$  heterojunction were taken to reveal the chemical valence state of components. From Fig. S5a, the XPS survey spectrum of  $\text{Bi}_4\text{MoO}_9$  showed the signals of Bi, Mo and O elements, while the Bi, Mo, O and Br signals could be clearly observed in the  $\text{BiOBr}/\text{Bi}_4\text{MoO}_9$  survey spectrum. No other elements were discerned, suggesting the high purity of catalysts. As shown in Fig. S5b, two featured peaks with the binding energy of 158.81 and 164.12 eV were consistent with the Bi 4f<sub>7/2</sub> and Bi 4f<sub>5/2</sub> of  $\text{Bi}^{3+}$  [1]. However, a shift of 0.15-0.25 eV toward the higher Bi 4f binding energies could be observed in the  $\text{BiOBr}/\text{Bi}_4\text{MoO}_9$  heterojunction, which might be due to the charge transfer caused by the strong interaction between  $\text{BiOBr}$  and  $\text{Bi}_4\text{MoO}_9$ . As presented in Fig. S5c, two main signals for Mo 3d<sub>5/2</sub> and Mo 3d<sub>3/2</sub> centered at 231.80 and 234.94 eV originated from oxidized  $\text{Mo}^{6+}$  [2]. Additionally, the Br 3d spectrum of  $\text{BiOBr}/\text{Bi}_4\text{MoO}_9$  (Fig. S5d) demonstrated the major peak at 68.28 and 69.30 eV, which could be assigned to the typical binding energy of  $\text{Br}^-$  ions [3].

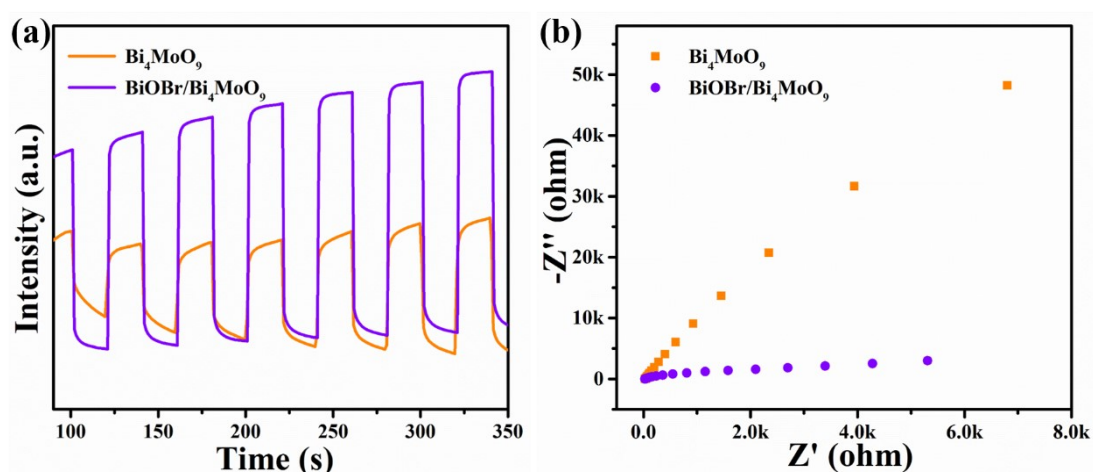


Fig. S6 (a) Plots of photocurrent density vs. irradiation time, and (b) EIS spectra of  $\text{Bi}_6\text{Mo}_2\text{O}_{15}$  and  $\text{BiOBr}/\text{Bi}_6\text{Mo}_2\text{O}_{15}$ .

To illustrate the reasons for the enhanced photocatalytic activity of the BiOBr/Bi<sub>4</sub>MoO<sub>9</sub> composite, the photocurrent-time measurement and EIS were exploited to characterize the Bi<sub>4</sub>MoO<sub>9</sub> and BiOBr/Bi<sub>4</sub>MoO<sub>9</sub> samples. As shown in Fig. S6a, the photocurrent density of BiOBr/ Bi<sub>4</sub>MoO<sub>9</sub> composite was much greater than that of Bi<sub>4</sub>MoO<sub>9</sub>, which indicated that more charge carriers in BiOBr/Bi<sub>4</sub>MoO<sub>9</sub>. Fig. S6b describes the EIS Nyquist plots of Bi<sub>6</sub>Mo<sub>2</sub>O<sub>15</sub> and BiOBr/Bi<sub>4</sub>MoO<sub>9</sub>. It could be seen that the diameter of the arc radius for the BiOBr/Bi<sub>4</sub>MoO<sub>9</sub> sample was smaller than Bi<sub>4</sub>MoO<sub>9</sub>. These results showed that the formation of BiOBr/ Bi<sub>4</sub>MoO<sub>9</sub> heterojunction inhibited the recombination of photogenerated carriers, which was conducive to the separation and transfer of photogenerated carriers in photocatalytic reaction.

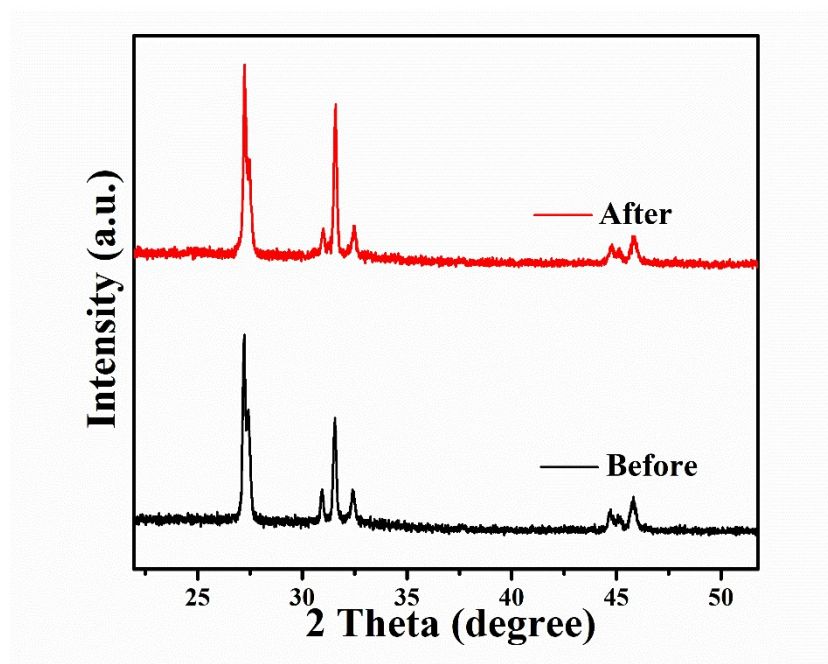


Fig. S7 (a) XRD patterns of BiOBr/Bi<sub>4</sub>MoO<sub>9</sub> before and after the photocatalytic reaction.

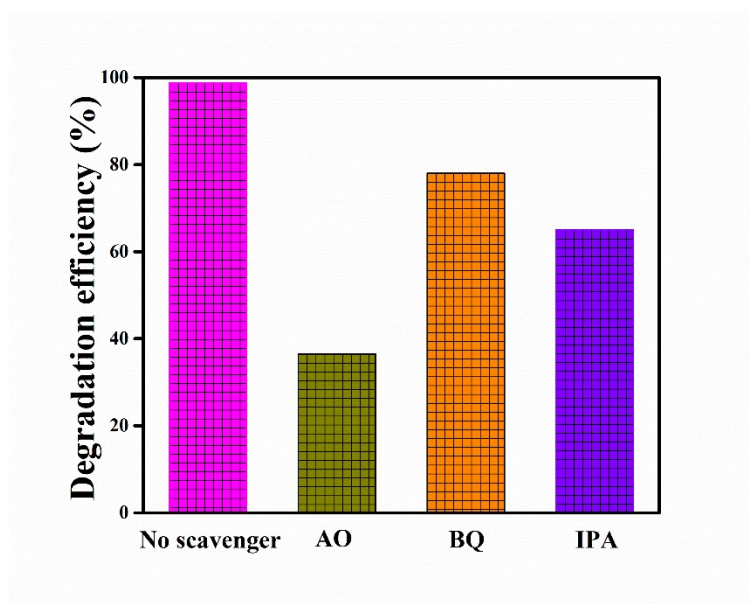


Fig. S8 Influence of various scavengers on the visible light photocatalytic activity of BiOBr/Bi<sub>4</sub>MoO<sub>9</sub> photocatalyst.

To elucidate the photocatalytic mechanism of the BiOBr/Bi<sub>4</sub>MoO<sub>9</sub> heterojunction on the degradation of TC during the photocatalytic process, ammonium oxalate (AO,  $h^+$  quencher), 1, 4-benzoquinone (BQ,  $\cdot O_2^-$  quencher) and isopropanol (IPA,  $\cdot OH$  quencher) were chosen to be scavengers in the degradation experiment of TC. As shown in Fig. S8, the degradation percentages of TC rapidly descended in the presence of AO, which indicates that  $h^+$  were the main active species to oxidize the TC pollutants. Besides, it was clearly observed that the photocatalytic degradation percentages of BiOBr/Bi<sub>4</sub>MoO<sub>9</sub> have been slightly changed with the addition of BQ and IPA, demonstrating that the  $\cdot O_2^-$  and  $\cdot OH$  played an assistant role in the photocatalytic degradation of TC. In addition, it seemed that the CB potentials of Bi<sub>4</sub>MoO<sub>9</sub> were not negative enough to reduce O<sub>2</sub> to  $\cdot O_2^-$  radicals because the O<sub>2</sub>/ $\cdot O_2^-$  potential (-0.33 eV) is more negative than CB potential of Bi<sub>4</sub>MoO<sub>9</sub> (-0.28 eV) yet, the higher energy part of Bi<sub>4</sub>MoO<sub>9</sub> (or BiOBr) can induce the photoexcited electrons



exciting up to a reformed higher CB potential more negatively than standard redox potential of  $O_2/\cdot O_2^-$  under visible light irradiation. Accordingly,  $\cdot O_2^-$  still could generate by the reduction of  $O_2$ .

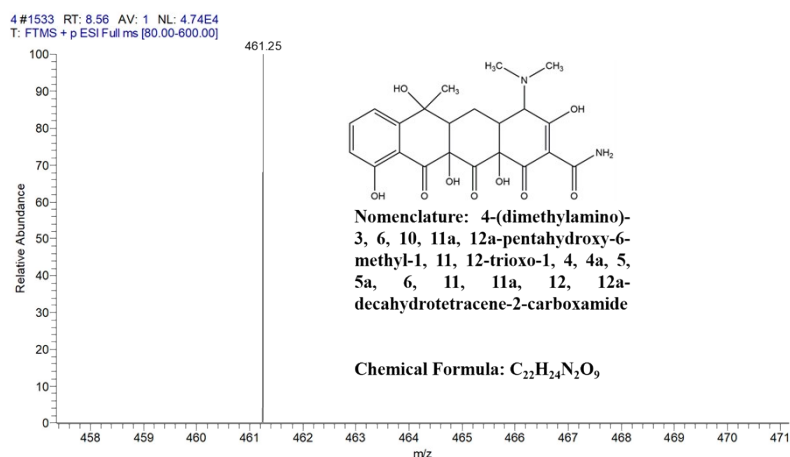


Fig. S9 The MS of TC (I) [ $m/z = 461$ ] and the naming of compound.

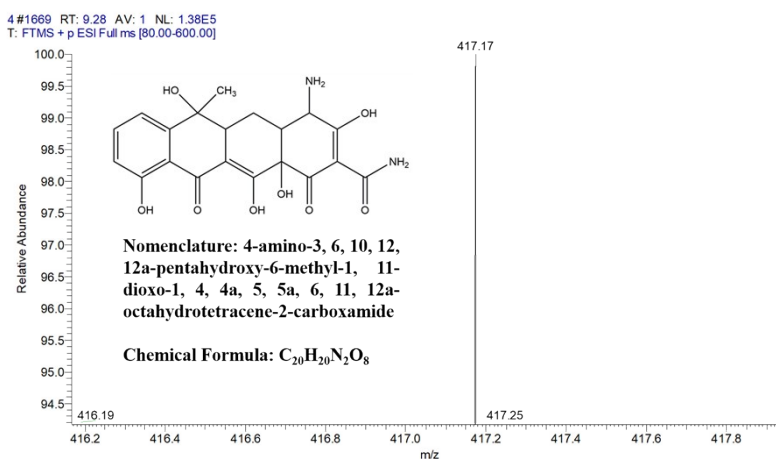


Fig. S10 The MS of TC (II) [ $m/z = 417$ ] and the naming of compound.

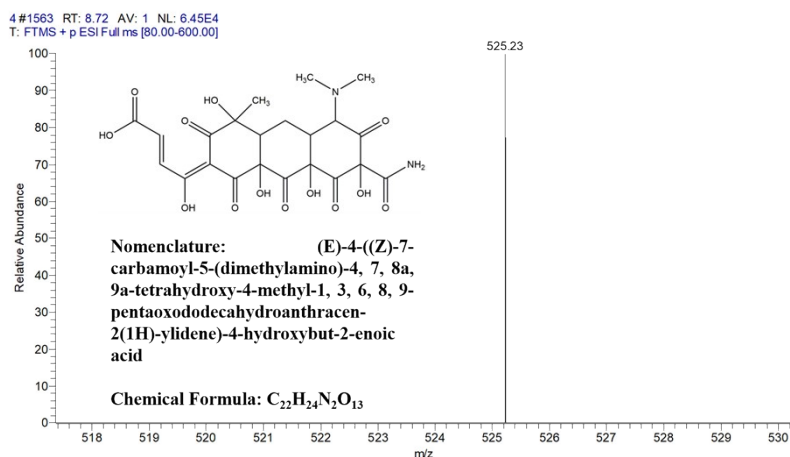


Fig. S11 The MS of TC (III) [ $m/z = 525$ ] and the naming of compound.

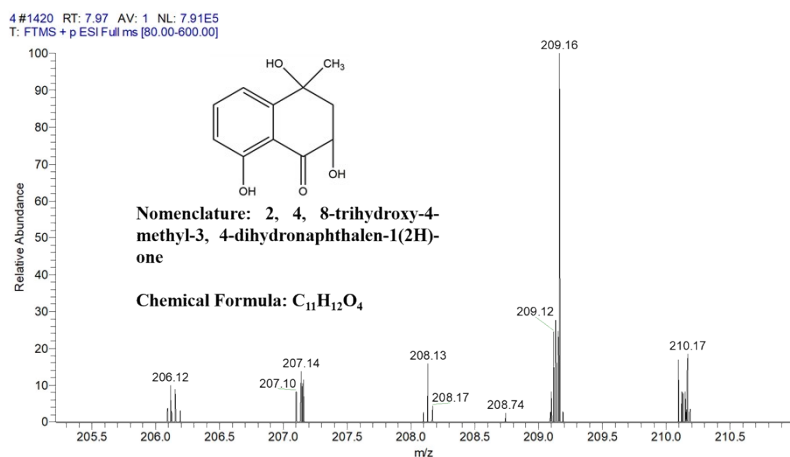


Fig. S12 The MS of TC (IV) [ $m/z = 209$ ] and the naming of compound.

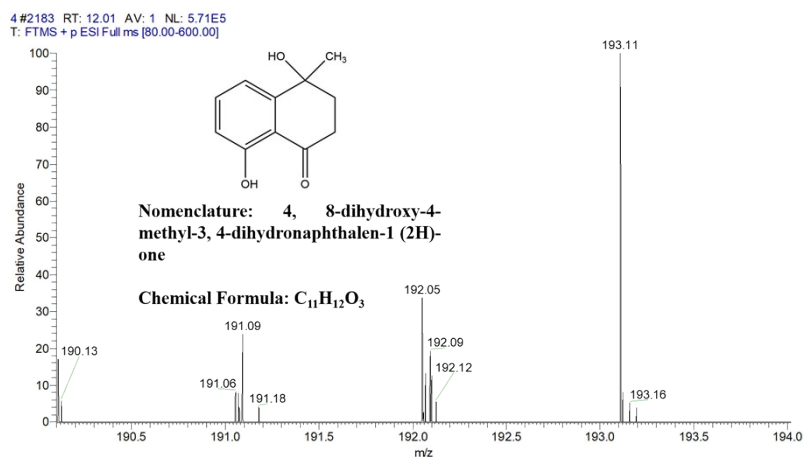


Fig. S13 The MS of TC (V) [ $m/z = 193$ ] and the naming of compound.

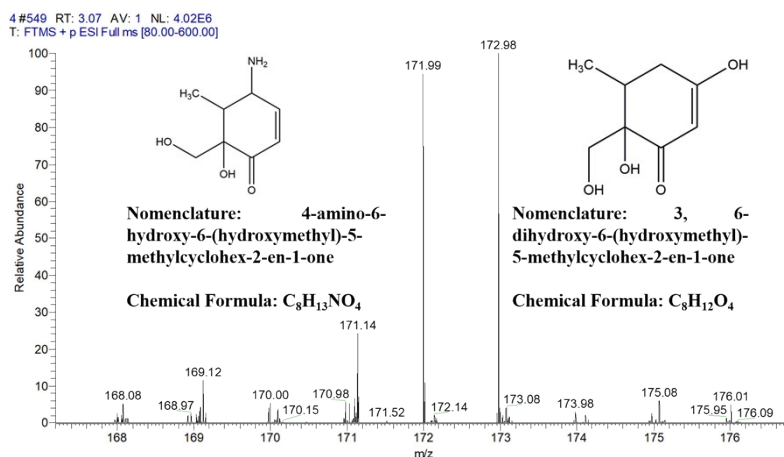


Fig. S14 The MS of TC (VI) [ $m/z = 173$ ], TC (VII) [ $m/z = 172$ ] and the naming of compound.

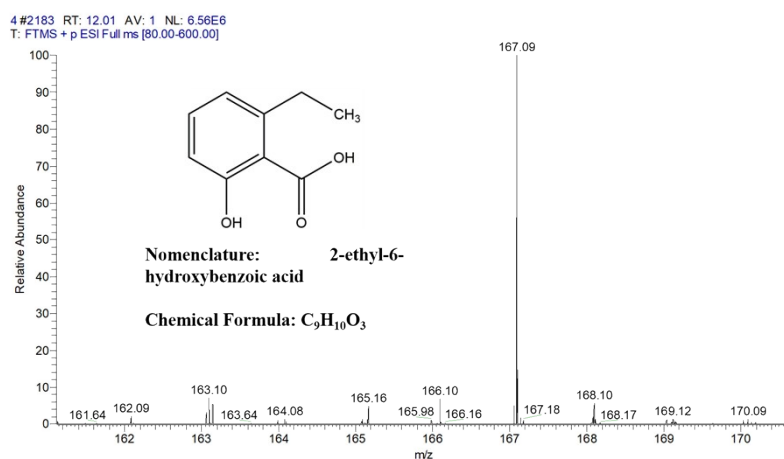


Fig. S15 The MS of TC (VIII) [ $m/z = 167$ ] and the naming of compound.

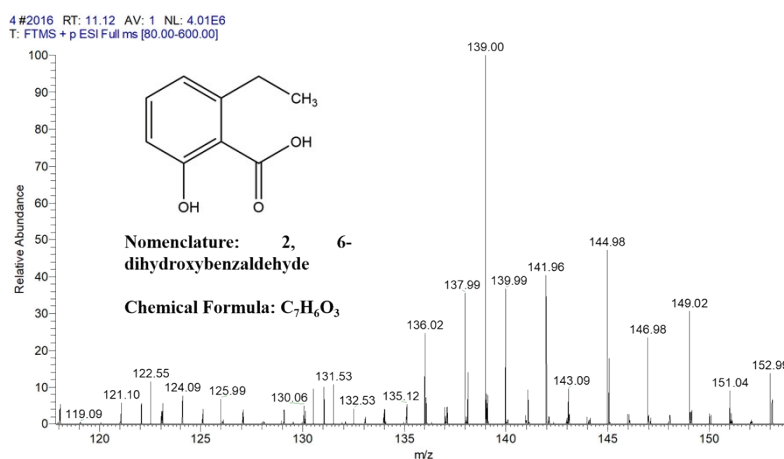
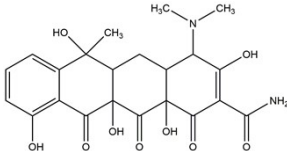
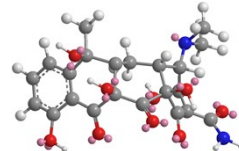
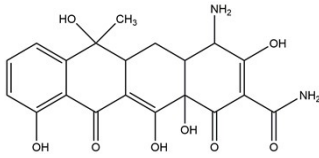
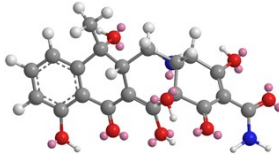
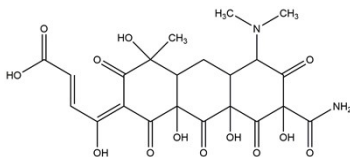
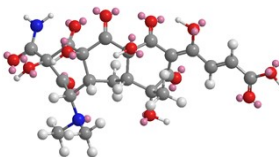
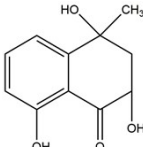
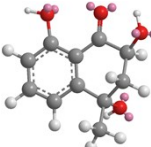
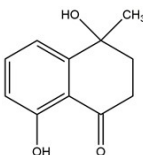
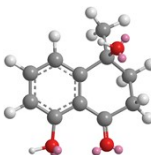


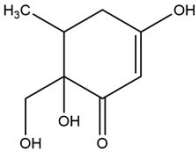
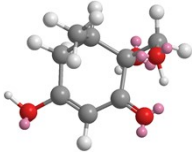
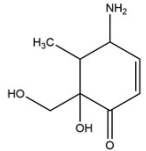
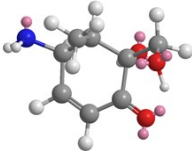
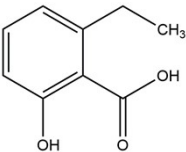
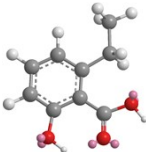
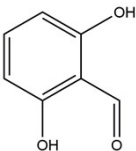
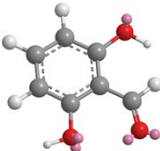
Fig. S16 The MS of TC (IX) [ $m/z = 139$ ] and the naming of compound.

**Table S1** The pseudo-first order rate constants  $k$  for TC photocomposition.

Sample	$k$ ( $\text{min}^{-1}$ )	Standard	Correlation
		error	coefficient R
<b>Bi<sub>4</sub>MoO<sub>9</sub></b>	0.00208	0.00010	0.9736
<b>BiOBr</b>	0.02563	0.00164	0.9971
<b>BiOBr/Bi<sub>4</sub>MoO<sub>9</sub></b>	0.00238	0.00238	0.9734

**Table S2** Possible degradation intermediates identified by LC-MS.

Retention time (min)	m/z	Possible structure	
8.56	461		
9.28	417		
8.72	525		
7.97	209		
12.01	193		

3.07	173		
3.07	172		
12.01	167		
11.12	139		

## Notes and references

- [1] J. Lv, K. Dai, J. Zhang, L. Geng, C. Liang, Q. Liu, G. Zhu, C. Chen, Facile synthesis of Z-scheme graphitic-C<sub>3</sub>N<sub>4</sub>/Bi<sub>2</sub>MoO<sub>6</sub> nanocomposite for enhanced visible photocatalytic properties, *Appl. Surf. Sci.*, 358 (2015) 377-384.
- [2] Y. Chen, G. Tian, Y. Shi, Y. Xiao, H. Fu, Hierarchical MoS<sub>2</sub>/Bi<sub>2</sub>MoO<sub>6</sub> composites with synergistic effect for enhanced visible photocatalytic activity, *Appl. Catal. B: Environ.*, 164 (2015) 40-47.
- [3] L. Ruan, J. Liu, Q. Zhou, J. Hu, G. Xu, X. Shu, Y. Wu, A flake-tube structured BiOBr-TiO<sub>2</sub> nanotube array heterojunction with enhanced visible light photocatalytic activity, *New J. Chem.*, 38 (2014) 3022-3028.